Probing the surface phase diagram of $Fe_3O_4(001)$ towards the Fe-rich limit: Evidence for progressive reduction of the surface

Zbynek Novotny,[1] Narasimham Mulakaluri,[2] Zoltan Edes,[1,3] Michael Schmid,[1] Rossitza Pentcheva,[2] Ulrike Diebold,[1] and Gareth S. Parkinson[1,*]

[1]*Institute of Applied Physics, Vienna University of Technology, Wiedner Hauptstrasse 8-10/134, 1040 Vienna, Austria*
[2]*Department of Earth and Environmental Sciences, University of Munich, Theresienstrasse 41, 80333 Munich, Germany*
[3]*CEITEC BUT, Technicka 10, 61669 Brno, Czech Republic*

(Received 5 February 2013; published 8 May 2013; corrected 1 July 2013)

Reduced terminations of the $Fe_3O_4(001)$ surface were studied using scanning tunneling microscopy, x-ray photoelectron spectroscopy (XPS), and density functional theory (DFT). Fe atoms, deposited onto the thermodynamically stable, distorted B-layer termination at room temperature (RT), occupy one of two available tetrahedrally coordinated sites per $(\sqrt{2} \times \sqrt{2})R45^\circ$ unit cell. Further RT deposition results in Fe clusters. With mild annealing, a second Fe adatom per unit cell is accommodated, though not in the second tetrahedral site. Rather both Fe atoms reside in octahedral coordinated sites, leading to a "Fe-dimer" termination. At four additional Fe atoms per unit cell, all surface octahedral sites are occupied, resulting in a FeO(001)-like phase. The observed configurations are consistent with the calculated surface phase diagram. Both XPS and DFT + U results indicate a progressive reduction of surface iron from Fe^{3+} to Fe^{2+} upon Fe deposition. The antiferromagnetic FeO layer on top of ferromagnetic $Fe_3O_4(001)$ suggests possible exchange bias in this system.

DOI: 10.1103/PhysRevB.87.195410 PACS number(s): 68.37.Ef, 68.47.Gh, 68.43.Bc

I. INTRODUCTION

Iron, the fourth most abundant element in the Earth's crust, is oxidized under ambient conditions forming several stable Fe oxides and hydroxides.[1] The Fe oxides differ in the concentration, distribution, and oxidation state of Fe cations in interstitial sites of a close-packed oxygen anion lattice.[1] Under oxidizing conditions, hematite (α-Fe_2O_3) and maghemite (γ-Fe_2O_3) are stable phases; Fe^{3+} occupy both octahedral (Fe-O_6) and tetrahedral (Fe-O_4) coordinated sites in maghemite, and octahedral sites in hematite. Under reducing conditions wustite (FeO) is formed, in which Fe^{2+} cations occupy octahedral coordinated sites. Magnetite (Fe_3O_4) represents the stable intermediate case, with both Fe^{3+} and Fe^{2+} cations present in an inverse-spinel structure [standard formula AB_2O_4; see Fig. 1(a)]. Fe^{3+} cations (denoted FeA; blue in Fig. 1) occupy one-eighth of the tetrahedral sites, while a 1:1 mixture of Fe^{2+} and Fe^{3+} fills half of the octahedral sites (FeB, yellow). The mixed valence of Fe_3O_4 leads to several interesting and useful phenomena including ferrimagnetism[1] and redox surface chemistry,[2] while band structure calculations predict room-temperature half-metallicity.[3] The surface properties play an important role in many applications including geochemistry, corrosion science, weathering, biomedicine, and heterogeneous catalysis.[1,4–6]

At the $Fe_3O_4(111)$ surface, three distinct terminations are observed, exposing either a close-packed oxygen plane, FeA, or FeB atoms.[7] Which of these terminations is manifested is highly dependent on the sample preparation conditions and multiple terminations can exist concurrently,[6–9] making quantitative interpretation of data from surface averaging techniques difficult. The oxygen termination has been shown to be inert toward adsorbates such as H_2O and CCl_4, whereas cation terminations introduce reactivity.[8,9]

For the (001) surface, early work proposed surface terminations with ordered oxygen vacancies or Fe adatoms, partly to explain the $(\sqrt{2} \times \sqrt{2})R45^\circ$ symmetry observed in low-energy electron diffraction (LEED) images,[10–12] and partly to satisfy charge compensation arguments. From a purely ionic point of view, $Fe_3O_4(001)$ is a Tasker type 3 surface,[13] and thus significant reconstruction is expected.[14] However, such considerations are not necessarily valid for Fe_3O_4, which is metallic at RT. It has since been established that a nominally polar B-layer termination is energetically favorable over a wide range of O chemical potentials[15–17] [top surface in Fig. 1(a); top view shown in Fig. 1(b)]. This surface is stabilized by a subtle lattice distortion (lateral relaxations of the order 0.1 Å), and theoretical calculations (DFT + U) predict coupling of the lattice strains to subsurface charge and orbital order.[15–17] The model is consistent with undulating rows of FeB(S) atoms observed in scanning tunnelling microscopy (STM) images,[10,18,19] the surface band gap of 0.2 eV,[20] and the structure of surface antiphase domain boundaries.[21] In what follows, the label (S) denotes atoms in the surface layer and (S-1) the first subsurface layer, including both FeA and FeB (see Fig. 1). The concentration of surface defects (Fe adatoms[22] and O vacancies[19]) on the sputter-annealed-oxidized surface of a single crystal is typically less than 1% under ultrahigh vacuum (UHV) conditions.

In a recent publication[22] we reported a metastable 0.5 ML FeA termination, in which Fe atoms occupy FeA-like sites consistent with a continuation of the bulk structure. The FeA(S) site, labeled n in Fig. 1(b), is twofold coordinated to O(S) atoms. In the bulk, FeA atoms are fourfold coordinated [see Fig. 1(a)]. Reduction of the surface was achieved through the preferential removal of oxygen during Ar^+ bombardment, a procedure that led to a significant roughening of the surface, making it difficult to image using STM. However, small areas

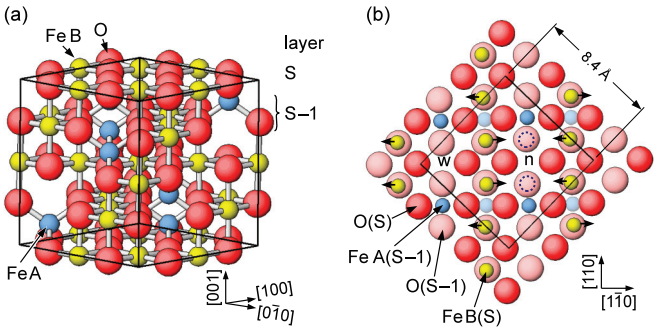

FIG. 1. (Color online) (a) Inverse spinel bulk unit cell of Fe_3O_4. In the (001) direction planes comprising tetrahedrally coordinated FeA atoms (A layer) alternate with planes containing octahedral FeB atoms and oxygen atoms (B layer). (b) Top view of the distorted B-layer termination of $Fe_3O_4(001)$ as determined by DFT + U calculations. In-plane relaxations perpendicular to the surface FeB(S) row direction lead to a $(\sqrt{2} \times \sqrt{2})R45^\circ$ symmetry (black square). The two bulk-continuation FeA(S) sites within the reconstructed unit cell are rendered inequivalent by the reconstruction [sites labeled narrow "*n*" and wide "*w*," where the O-O distance in the surface is compressed (3.27 Å) and expanded (3.44 Å), respectively]. Two dark blue broken circles indicate the octahedral sites in the oxygen lattice occupied by Fe atoms in the Fe-dimer termination.

appeared to exhibit so-called "Fe-dimers."[12,17,23] Since the Fe dimer was centered on the same $(\sqrt{2} \times \sqrt{2})R45^\circ$ sublattice as the FeA(S) protrusions, we proposed the Fe dimer to straddle the FeA(S) site [i.e., Fe atoms occupy positions on either side of the *n* site, as indicated by the dark blue broken circles in Fig. 1(b)], rather than straddle a subsurface FeA(S-1) site as suggested previously.[12,17,23] Heating above 500 °C, the surface was reoxidized via bulk-surface diffusion and the distorted B-layer termination with larger terraces was recovered.

In this paper we investigate the surface phase diagram of $Fe_3O_4(001)$ towards the Fe-rich limit by directly depositing Fe onto the distorted B-layer surface. This procedure allows tight, reproducible control of the surface stoichiometry, while maintaining the large terraces of the as prepared distorted B-layer surface. Using this approach we synthesize several stable reduced terminations, including a complete Fe-dimer termination and an FeO(001)-like termination. XPS measurements and DFT + U calculations show that the Fe-rich surface phases contain mainly Fe^{2+}. DFT + U calculations provide insight on the energetic stability of the experimentally observed configurations and their structural, electronic, and magnetic properties. In particular, we show that the "Fe dimer" is the result of a conversion from tetrahedral to octahedral coordination, and that no Fe-Fe bond is formed.

II. EXPERIMENTAL AND COMPUTATIONAL DETAILS

STM and x-ray photoelectron spectroscopy (XPS) experiments were conducted in an ultrahigh vacuum (UHV) system, consisting of two vessels for sample preparation and analysis, with a base pressure of 1×10^{-10} mbar and 7×10^{-11} mbar, respectively. STM measurements were carried out with electrochemically etched W tips in the constant-current mode imaging empty states at room temperature (RT) ($V_{sample} = +0.6$ to $+1.2$ V and $I_{tunnel} = 0.2$ to 0.36 nA). A synthetic $Fe_3O_4(001)$ single crystal was used in this study, cut and polished by MaTeck GmbH from a single crystal bar grown using the floating zone method by Mao and co-workers at Tulane University.[24] The distorted B-layer termination was prepared *in situ* by cycles of Ar^+ sputtering (1 keV; $I_{sample} = \sim 1$ μA), followed by annealing at 923 K for 1 h in 2×10^{-6} mbar O_2 backpressure. The annealing was performed by electron beam bombardment of the backside of the Mo sample plate. Fe was evaporated from a 2-mm-thick rod (99.99 + %, MaTeck GmbH), heated by electron bombardment; the amount of evaporated material was calibrated by a quartz crystal microbalance, and for very low Fe coverages, by STM. The Fe deposition rate was 0.05 ML/s, where 1 ML is defined as two extra atoms per $(\sqrt{2} \times \sqrt{2})R45^\circ$ unit cell or 2.84×10^{14} atoms/cm^2. This definition is chosen since two Fe atoms per unit cell are equivalent to a bulk truncation at the A layer [see Fig. 1(a)]. During deposition, the pressure in the preparation chamber was in the low 10^{-9} mbar range. Fe deposition was done at RT and 573 K, measured using a calibrated IR pyrometer.

Density functional theory (DFT) calculations were performed using the FP-LAPW (full potential linear augmented plane wave) method in the WIEN2k[25] implementation. The generalized gradient approximation (GGA)[26] of the exchange-correlation potential is used. The influence of electronic correlations beyond GGA is considered within the LDA/GGA + U[27] method, applying $U = 5$ eV and $J = 1$ eV, similar to values used for bulk Fe_3O_4.[28,29] The surfaces are modeled using symmetric slabs containing seven B and six A layers with additional iron deposited on the surface depending on the coverage. The slabs are separated by at least 10 Å from their periodic images to avoid spurious interactions. For further details on the calculations the reader is referred to Refs. 16,30 and 31.

III. RESULTS

A. Fe-rich terminations of the $Fe_3O_4(001)$—Structure

Figure 2 shows the surface phase diagram of $Fe_3O_4(001)$ obtained in the framework of *ab initio* atomistic thermodynamics.[32] Over a broad range of oxygen chemical potentials the phase diagram is dominated by the distorted B-layer termination [see Fig. 1(b)], as reported previously.[16,17] Under reducing conditions ($-2.89 < \mu_0 < -2.44$) a surface termination with oxygen vacancies (B + V_O) and a B layer with additional tetrahedral Fe in every second surface site (0.5 ML FeA termination) are predicted to compete with a difference in stability of (0.7–2.9) meV/Å^2. Towards the Fe-rich limit, the DFT calculations show that our model of the 1 ML Fe-dimer termination (which differs from that considered in prior studies) is energetically favorable over a 1 ML FeA termination. As demonstrated below, the "Fe dimer" arises from a switching of the cation coordination from tetrahedral to octahedral; no direct Fe-Fe bond is formed [see Fig. 4(c)]. At the lowest oxygen chemical potential, Fe atoms occupy all octahedral sites and an FeO-like layer is stabilized [see Fig. 5(b)].

In experiment, isolated Fe adatoms, deposited at RT, occupy FeA(S)-like sites as expected on the basis of our previous observations.[22] Figure 3(a) shows an STM image acquired

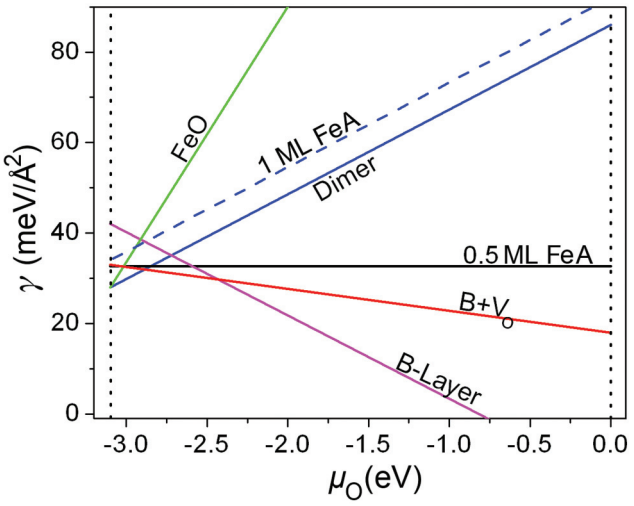

FIG. 2. (Color online) Surface phase diagram of $Fe_3O_4(001)$ derived from the DFT + U calculations. For each value of the oxygen chemical potential μ_O, the lowest line shows the most favorable surface termination. The distorted B-layer is stable over a broad range of oxygen chemical potentials. In a narrow range towards oxygen poor conditions (low μ_O) the B-layer competes with oxygen vacancies ($B + V_O$) and a 0.5 ML FeA layer, followed by a Fe dimer termination and, finally, by an FeO termination. Chemical potentials beyond the broken lines correspond to formation of metallic Fe (left) and condensation of oxygen (right).

after deposition of 0.025 ML Fe on the distorted B layer at RT. The characteristic undulating FeB(S) rows of the substrate are clearly observed.[10,18,19,22] Hydroxyl groups [elongated protrusions on the FeB(S) row[18,19]], formed via highly efficient dissociation of water in the surface oxygen vacancies,[19] occur with similar coverage to a freshly prepared distorted B-layer surface. The deposited Fe atoms appear as 0.025 ML bright protrusions between the FeB(S) rows[22] [see the yellow circles in Fig. 3(a)]. In the inset of Fig. 3(a) we show a high-resolution STM image of one such protrusion. All FeA atoms occupy the narrow n site, as found previously for other adsorbates such as H,[18,19] Au,[33] and Pd.[34] Diffusion of the surface FeA(S) is rare at RT, but was observed occasionally between neighboring n sites along the FeB row direction.

For Fe coverages in excess of ~0.5 ML at RT, Fe clusters appear. Figure 3(b) shows an STM image following deposition of 0.8 ML Fe at RT. The FeB(S) rows of the distorted B-layer remain visible, together with FeA(S) atoms and large bright features attributable to Fe clusters. The inset shows a zoomed area with a low density of clusters, in which the cyan grid indicates the $(\sqrt{2} \times \sqrt{2})R45^\circ$ symmetry of the substrate, with the nodes centered at w sites. FeA(S) adatoms appear between the rows with a minimum separation of 11.9 Å along the row. Thus, even at this high Fe coverage, only one of the two available FeA(S) sites per unit cell is occupied. This indicates that the 0.5 ML FeA termination is the most reduced, stable termination achievable at RT. DFT + U calculations for a complete 0.5 ML FeA structure [one additional FeA within a $(\sqrt{2} \times \sqrt{2})R45^\circ$ supercell] reveal that the Fe adatom relaxes strongly inward relative to the bulk FeA(S) position (relative height with respect to the surface oxygen is only 0.45 Å

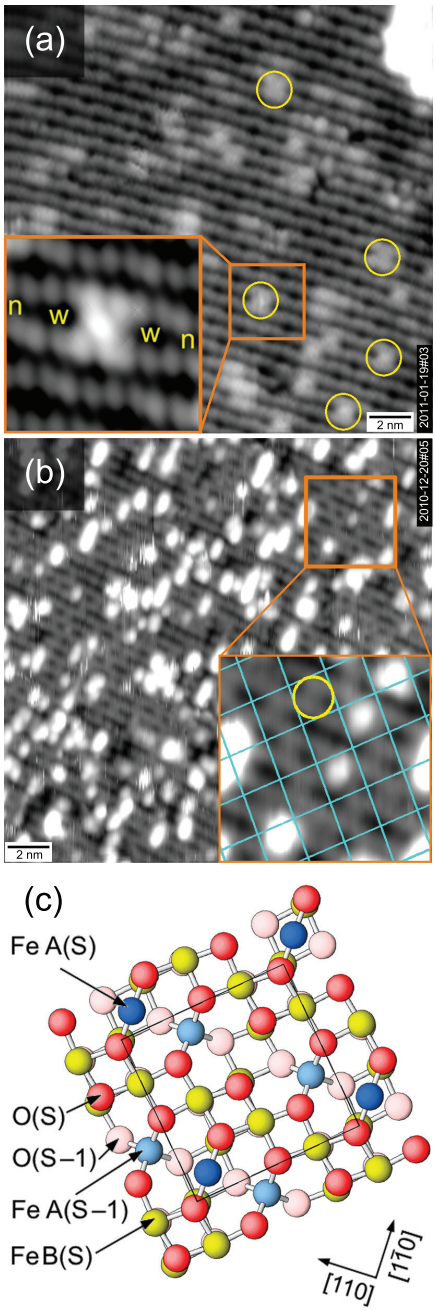

FIG. 3. (Color online) Deposition of Fe on the $Fe_3O_4(001)$ surface at RT. (a) STM image (20 × 20 nm^2, $V_{sample} = +1.2$ V, $I_{tunnel} =$ 0.3 nA) after deposition of 0.025 ML Fe at RT. Adsorbed Fe atoms, marked by yellow circles, occupy FeA bulk continuation sites between the FeB rows. The inset shows a high-resolution image (2.7 × 2.7 nm^2, +0.9 V/0.36 nA) of an FeA adatom adsorbed in the site labeled n in Fig. 1(b). (b) STM image (20 × 20 nm^2, +1.2 V/0.3 nA) after deposition of 0.8 ML Fe at RT. FeA adatoms and Fe clusters are observed. The inset shows a high-resolution STM image of the area marked by the orange square, with one FeA indicated by the yellow circle. FeA adatoms occupy positions consistent with $(\sqrt{2} \times \sqrt{2})R45^\circ$ symmetry (cyan grid, nodes centered at w sites). (c) Structural model of the 0.5 ML FeA termination derived from DFT + U calculations. The FeA adatom is twofold coordinated to surface O atoms. The O-O distance increases to accommodate the extra Fe atom, which relaxes into the surface by 0.62 Å relative to the bulk spacing.

compared to 1.07 Å in a truncated bulk), causing the neighboring oxygen atoms to relax away to a separation of 3.63 Å (bulk separation = 2.85 Å). The neighboring FeB(S) atoms also relax away from the FeA(S), increasing their separation to 6.21 Å (bulk separation = 5.94 Å). This configuration, in which the FeA(S) atom relaxes into the surface and the neighboring atoms relax away in the plane, was obtained irrespective of whether the additional Fe atom is initially placed at either the *n* or *w* FeA site of the distorted B-layer surface.

The calculated surface phase diagram (Fig. 2) indicates that the Fe-dimer termination is favored over the 0.5 ML FeA termination in strongly reducing conditions, suggesting a thermal barrier inhibits its formation at RT. The surface shown in Fig. 4(a) (0.8 ML Fe deposited at RT) results from flash annealing the surface seen in Fig. 3(b) to 423 K. The FeB(S) rows of the underlying substrate remain visible and the number of Fe clusters is significantly reduced. Between the rows, single protrusions coexist with Fe dimers. In areas where the local Fe coverage is high (yellow rectangle, zoomed bottom right), Fe dimers are distributed with $(\sqrt{2} \times \sqrt{2})R45^\circ$ symmetry (cyan square). Where the coverage is locally lower (orange rectangle, zoomed top right), single Fe adatoms and Fe dimers coexist. Interestingly, the single protrusions in this structure occupy a tetrahedral position directly above a subsurface FeA(S-1) atom, and not an octahedral site.

Figure 4(b) shows an STM image acquired following deposition of 0.7 ML Fe onto the clean B-layer terminated surface, postannealed at 573 K for 15 minutes. Only Fe dimers are observed between the FeB(S) rows, distributed with $(\sqrt{2} \times \sqrt{2})R45^\circ$ symmetry. The inset shows an atomically resolved STM image in which the protrusions of the dimer appear directly between the FeB(S) atoms of the neighboring rows. Therefore, the atoms of the Fe dimer occupy a similar octahedral position to the FeB(S) atoms [broken dark blue circles in Fig. 1(b)]. DFT + U calculations for the Fe-dimer surface confirm the Fe atoms of the "dimer" to be fivefold coordinated to oxygen [see Fig. 4(c)], 0.54 Å above the fourfold hollow site with Fe-O bond lengths of 2.04 Å. Simultaneously, the O(S)-FeB(S) and O(S)-FeB(S-1) bond lengths of oxygen connected to the dimer elongate to 2.27 Å, while the O(S)-FeB(S)/O(S)-FeB(S-1) bonds of undercoordinated oxygen are reduced (1.96 Å). The calculations indicate that no Fe-Fe bond is formed within the "Fe dimer." While another notation, e.g., "octahedral pair" would probably be a more accurate description of this motif, we continue to refer to this configuration as Fe dimers, in agreement with the nomenclature used in the literature.[12,23] As for the 0.5 ML FeA surface, the calculation converges to a similar final result

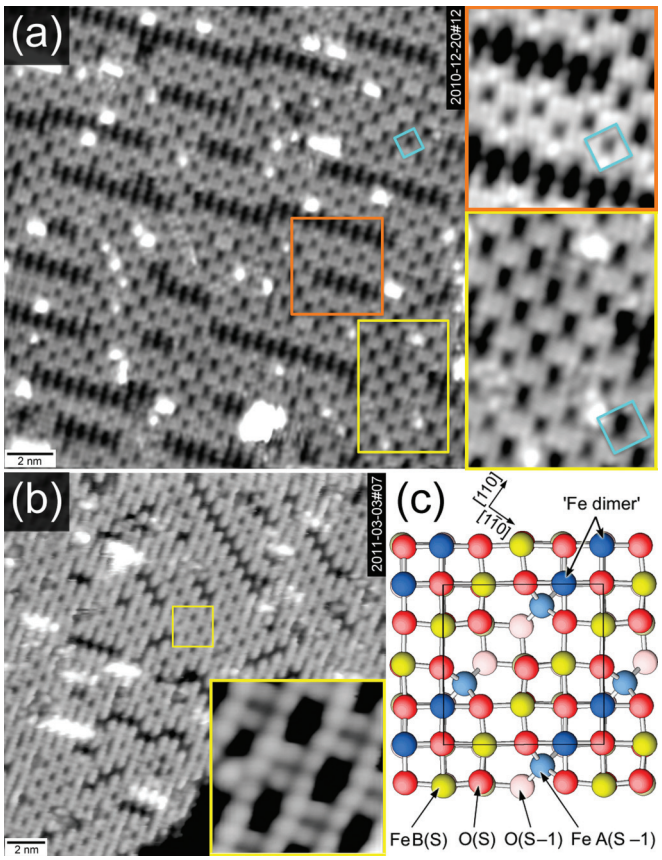

FIG. 4. (Color online) (a) STM image (20 × 20 nm^2, V_{sample} = +0.91 V, I_{tunnel} = +0.34 nA) following postannealing to 423 K of a surface containing 0.8 ML additional Fe, as also shown in Fig. 3(b). In areas of low local Fe coverage (orange rectangle, see inset for high resolution image), isolated Fe adatoms coexist with Fe dimers between the FeB(S) rows. In areas of high local Fe coverage (yellow rectangle, see inset for high resolution image), only Fe dimers are observed between the FeB(S) rows. (b) STM image (20 × 20 nm^2, +1.03 V/+0.32 nA) following deposition of 0.7 ML Fe onto the B-layer terminated surface at RT. The surface was postannealed at 573 K for 15 min. Only Fe dimers are observed between the FeB(S) rows. (inset) High resolution STM image of the area contained within the yellow rectangle in Fig. 3(b). Note that the atoms of the Fe dimer are located directly between FeB(S) atoms on neighboring FeB rows. (c) DFT + U derived model of the Fe dimer termination (top view).

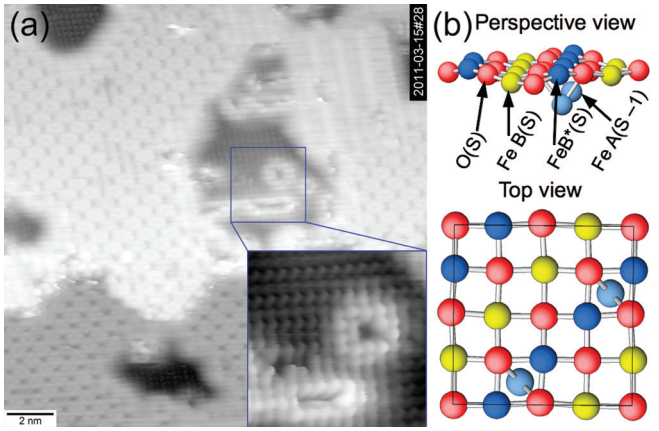

FIG. 5. (Color online) STM image (20 × 20 nm^2, V_{sample} = +0.65 V, I_{tunnel} = +0.32 nA) following deposition of 2 ML Fe at 573 K. The Fe-dimer termination coexists with an FeO-like termination. This appears as a square lattice as all octahedral interstitial sites in the O(S) lattice are filled (yellow and dark blue in model). The interface between the two regions is smooth, but the FeO-like areas contain many structural defects. (b) DFT + U derived structural model of a FeO(001)-like surface layer on the Fe_3O_4(001) bulk. Note that the FeB*(S) row with underlying FeA(S-1) neighbors (dark blue) is raised above the surface plane.

irrespective of whether the Fe atoms are initially placed in the *w* or *n* site.

Further deposition of Fe leads to the occupation of all octahedral sites in the surface oxygen lattice, and the formation of an FeO(001)-like surface layer. Figure 5(a), acquired following deposition of 2 ML Fe at 573 K, exhibits two distinct terminations. Some areas exhibit the Fe-dimer termination, as described above, while other areas exhibit a square lattice. The interface between the two regions is smooth and the FeB(S) rows are continuous over the boundary. This suggests occupation of the remaining two octahedral sites that remained empty in the Fe-dimer termination; such a surface layer has an FeO stoichiometry. The FeO-like areas contain significant structural defects, possibly related to the mismatch in the Fe-O bond length in FeO (2.17 Å) and Fe_3O_4 (2.14 Å). Note that the visible additional Fe is significantly less than the 2 ML nominally deposited. Most likely, some Fe diffuses into the subsurface or bulk of the sample when deposited at 573 K; Fe diffusion at this temperature was observed previously.[22]

The relaxed DFT + *U* structure of the FeO(001) termination in Fig. 5(b) reveals a strong buckling (0.48 Å) between the original FeB(S) rows and the additional FeB(S)-like atoms (hereafter denoted FeB*(S)). Along the surface FeB(S) rows a modulation of the FeB-FeB distance occurs in both the original and new FeB*(S) rows, with alternating shorter (2.87 Å) and longer (3.08–3.10 Å) bonds. The presence of the FeO layer pushes the subsurface FeA(S-1) towards the next B layer (S-1), resulting in shorter FeA(S-1)-O(S-1) bond lengths of 1.81 Å, and significantly longer ones to surface oxygen (2.36 Å). The O(S)-FeB(S-1) bond lengths are also elongated to ∼2.38–2.41 Å compared to 2.06 Å in bulk.

B. Fe-rich terminations of Fe_3O_4(001)—Electronic structure

In addition to the structural parameters, the DFT + *U* calculations reveal an interesting electronic structure. In Fig. 6 the total and projected density of states, split into majority

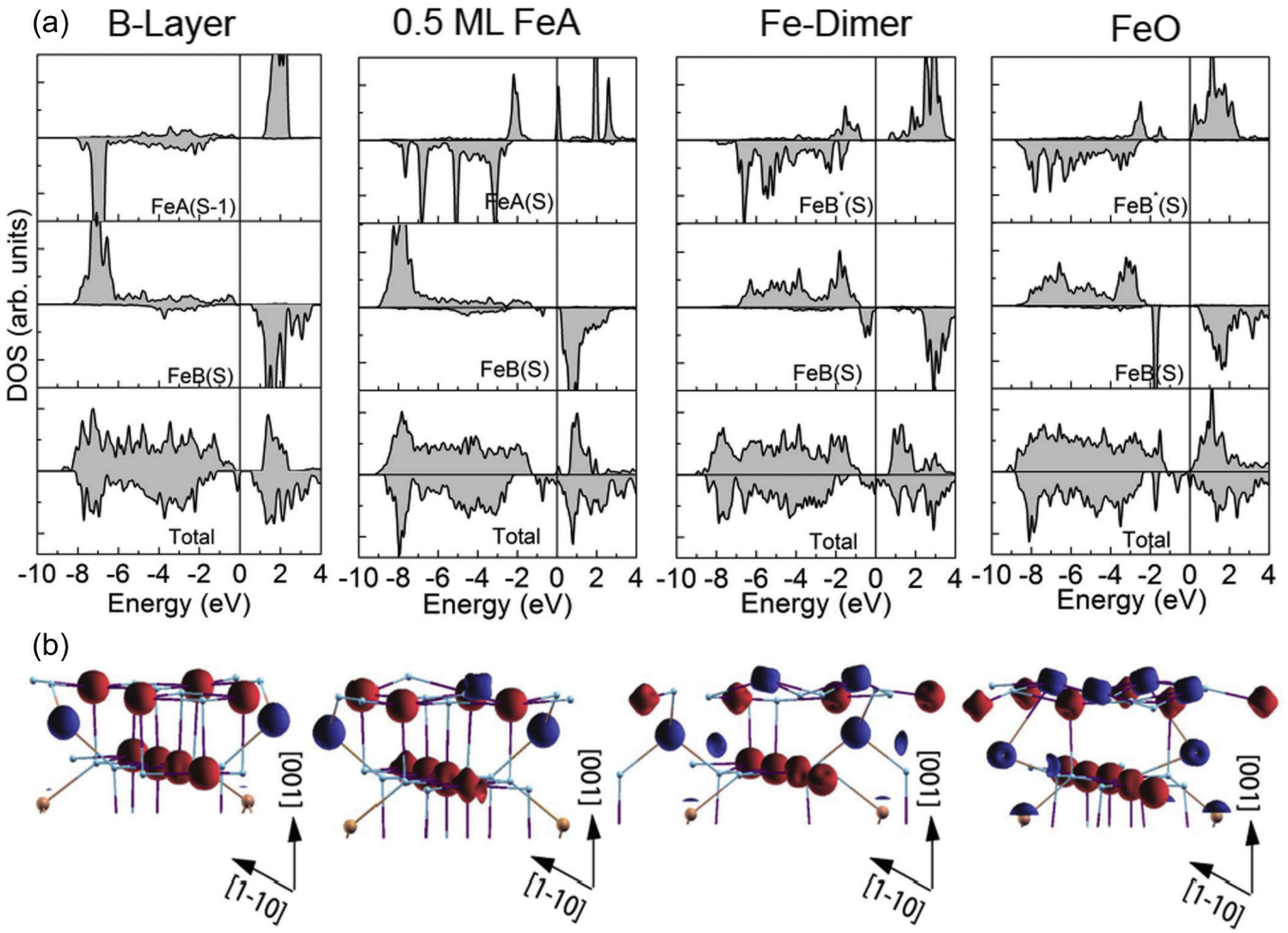

FIG. 6. (Color online) Density of states (DOS) and spin density for the surface terminations shown in Fig. 2. Top and middle panels show the partial density of states (PDOS) of surface and subsurface FeA and FeB 3*d* states, respectively. The bottom panels show the total DOS. While the surface layer remains insulating for all presented terminations (only for the 0.5 ML FeA structure there is a localized state pinned at E_F), half-metallic behavior is observed for all but the B-layer termination in the deeper layers due to incomplete charge localization. (b) Blue and red represent the two different spin orientations. A spherical spin distribution indicates an Fe^{3+} ion with a $3d^5$ occupation and deviations from the spherical shape indicates an Fe^{2+} with a $3d^6$ occupation. In the B-layer all FeB(S) are Fe^{3+}. With increasing Fe coverage a progressive reduction to Fe^{2+} takes place. Note that for the "Fe dimer" and FeO terminations the surface layer is completely Fe^{2+}.

and minority spin components, is plotted for each stable termination. In addition, a perspective view model of each configuration is presented, in which red and blue constant density contours denote the spin density of FeB and FeA respectively, with antiparallel magnetic moments. Deviations from the spherical spin density distribution (as in the high-spin $3d^5$ configuration of Fe^{3+}) indicate sites with Fe^{2+} character. Small, light blue spheres represent oxygen atoms. Consistent with previous theoretical and experimental results, the distorted B-layer termination is insulating[15,17,20] due to the charge and orbital ordering of Fe^{2+} and Fe^{3+} in the subsurface layers.[15,17] The surface FeB(S) [and FeA(S-1)] are exclusively Fe^{3+} [note the spherical spin density in Fig. 6(b)].[35] In the second B layer, in which the FeB(S-1) rows run at 90° to the surface rows, two distinct oxidation states are discerned: Fe^{3+}-like states, and those with a partial occupation of t_{2g} orbitals in the minority spin orientation (Fe^{2+}-like states). The different states are paired along the FeB(S-1) row, producing an overall $(\sqrt{2} \times \sqrt{2})R45°$ symmetry matched to the lattice distortion in the surface B layer. The orbital order leads to a half-metal to insulator transition in the surface.[15,17,30]

For the 0.5 ML FeA layer termination, a transition from insulating to half-metal character takes place (see total DOS). This is related to changes of the charge order in subsurface layers of the slab; the surface layers remain insulating. While in the B-layer termination, FeA(S-1) is Fe^{3+} with a fully occupied minority *d* band ($3d^5$ occupation), an additional state is occupied in the majority spin channel at the Fe adatoms, denoted FeA(S) in the 0.5 ML FeA layer, corresponding to a $3d^6$ (Fe^{2+}-like) state. A similar transition from insulating to half-metallic behavior was observed in previous studies upon hydrogen adsorption on $Fe_3O_4(001)$.[15,30,31]

In contrast to the B-layer and 0.5 ML FeA layer surfaces, in which FeB(S) are all Fe^{3+}, in the Fe-dimer and FeO terminations the FeB(S), FeB*(S) and FeA(S-1) atoms are reduced to Fe^{2+}. For the FeB(S) this comes from an additional electron in the minority spin channel below the Fermi level, while for the FeB*(S) and FeA(S-1) an additional orbital in the majority spin channel is occupied. Both exhibit a strong deviation from the spherical spin distribution [Fig. 6(b)]. The $FeO/Fe_3O_4(001)$ termination shows the largest gap in the surface layers, while states at the Fermi level originating from deeper layers lead to half-metallic behavior. The switch from tetrahedral (0.5 ML FeA) to octahedral (or fivefold) coordination (Fe dimer, FeO termination) leads to a change in crystal field splitting: the orbital character of the sixth electron in the 3*d* band changes from e_g character in 0.5 ML FeA to t_{2g} in both at the Fe-dimer and FeO terminations.

A further interesting feature is the magnetic order between the Fe ions. Different orientations of magnetic moments are indicated by red and blue spin densities in Fig. 6(b). In bulk Fe_3O_4, FeA and FeB spins couple antiferromagnetically, leading to a ferrimagnetic ground state. The additional octahedrally coordinated FeB*(S) in the Fe-dimer and FeO terminations align antiparallel to the original FeB(S) rows, consistent with the G-type magnetic order in FeO. This indicates that these reduced FeO/Fe_3O_4 surfaces may host interesting phenomena such as exchange bias.

The progressive surface reduction upon Fe deposition is visible in photoelectron spectroscopy. In Fig. 7 we show Fe

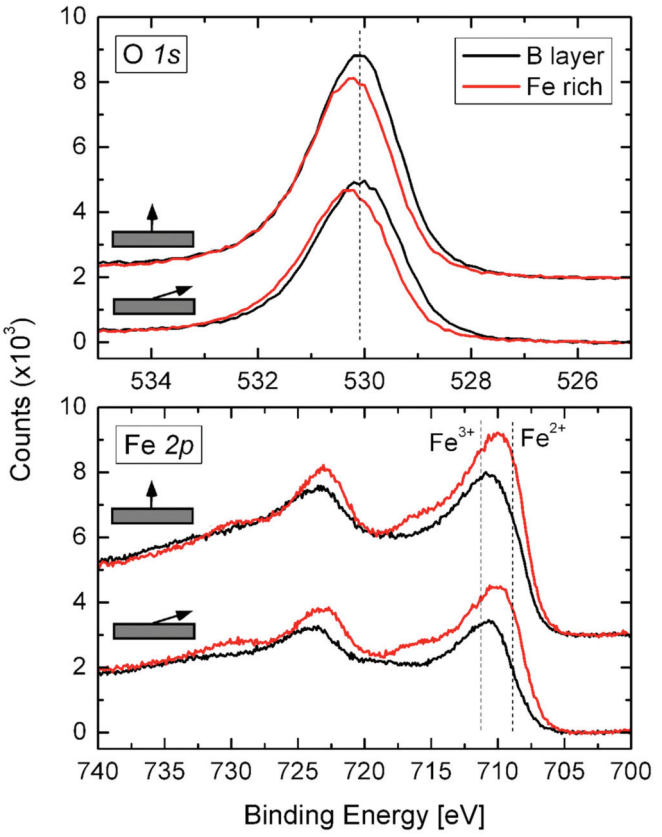

FIG. 7. (Color online) XPS for the O *1s* (top) and Fe *2p* (bottom) data acquired from a pure B-layer termination and a surface containing a high coverage of Fe dimers at both normal and grazing emission. The O *1s* peak is reduced in intensity and shifted slightly to higher binding energy (0.2 eV) for the surface with Fe dimers. The Fe $2p_{3/2}$ peak is shifted to lower binding energy and exhibits a satellite peak at 717 eV, consistent with an enhancement in Fe^{2+} cations. The effect is more pronounced at grazing emission, indicating that the additional Fe^{2+} is located at or near the surface.

2p and O *1s* XPS spectra, acquired with nonmonochromatized Al $K\alpha$ excitation, for the distorted B-layer termination and the Fe-dimer terminated surface. The data were acquired at normal emission, and 60° from normal emission to be more sensitive to changes in the surface layer(s). The O *1s* peak for the B layer appears as reported previously[18] with a binding energy of 530 eV with a slight asymmetry to the high binding energy side.[36] The O *1s* peak for the Fe-dimer terminated surface shifts 0.2 eV to higher binding energy. The Fe *2p* region has contributions from Fe^{3+} and Fe^{2+} cations at 711.4 eV and 709 eV, respectively.[37] The dominant contribution to the spectrum for the distorted B-layer surface comes from Fe^{3+} cations, since only this oxidation state is present in the surface layer,[15] while the second B-layer is an ordered 50:50 mix of 2+ and 3+ like states. The Fe *2p* spectrum for the Fe-dimer terminated surface is significantly more intense than the B layer, as expected since it contains additional Fe atoms. Furthermore, the Fe $2p_{3/2}$ peak is shifted to lower binding energy and the shakeup satellite feature at 717 eV[37] is enhanced. Both phenomena are consistent with an increase in the Fe^{2+} component in the surface layer.

IV. DISCUSSION

The results reported here clearly demonstrate the stability of Fe-rich terminations at the $Fe_3O_4(001)$ surface. For RT Fe deposition, tetrahedral coordination of surface Fe is preferred (Fig. 3), in keeping with the bulk structure. At low coverage, surface Fe atoms exclusively occupy the *n* site within the distorted B layer (see Fig. 1), maintaining the $(\sqrt{2} \times \sqrt{2})R45^\circ$ symmetry of the underlying B layer (0.5 ML FeA termination; see Fig. 3). However, the DFT + *U* calculations show that incorporation of the excess FeA(S) atom leads to an increased separation of the neighboring O(S) and FeB(S) atoms; thus, essentially, the Fe atom creates its own local *w* site, allowing it to relax toward the surface. Above 0.5 ML coverage, Fe clusters form. This suggests that occupation of the second vacant tetrahedral site of the clean B layer [see Fig. 1(a)] is highly unfavorable. This behavior is consistent with the instability of a 1 ML FeA termination predicted by the DFT calculations (see Fig. 2). A similar strong preference for the narrow FeA(S) site leads to the adatom templating observed for H,[18,19] Au,[33] and Pd[34] atoms at the $Fe_3O_4(001)$ surface, and an unusual adsorption mode for water that results in room temperature water splitting.[19]

Annealing the surface to 423 K facilitates a conversion from tetrahedral to octahedral Fe coordination. At 1 ML Fe coverage, the Fe-dimer structure, which also exhibits $(\sqrt{2} \times \sqrt{2})R45^\circ$ symmetry, becomes stable. Only at the highest coverage studied (2 ML Fe) is this symmetry modified; the vacant octahedral sites between the Fe dimers are filled, producing the FeO termination. It is important to note that it is impossible to distinguish the distorted B-layer, the 0.5 ML FeA, and Fe-dimer terminations by qualitative LEED. The same would also be true of the B-V_O termination predicted by theory[30] (see Fig. 2); however, despite extensive attempts to produce such a surface by variation of the preparation conditions, a surface with a high concentration of oxygen vacancies has never been observed experimentally. In the absence of STM, some information about the surface Fe content can be garnered from Fe *2p* XPS spectra, since all Fe terminations containing additional undercoordinated Fe atoms exhibit an additional Fe^{2+} shoulder relative to the distorted B layer (see Fig. 7), although the relatively broad XPS peaks for the various Fe oxidation states makes a clear identification not straightforward.[37]

Diffusion of isolated Fe adatoms in tetrahedral sites at RT [as seen in Fig. 3(a)] is extremely rare, but is observed occasionally between neighboring *n* sites along the FeB row direction in STM "movies," where several sequential images were acquired from the same sample area (not shown). After annealing at 423 K (Fig. 4), Fe dimers coexist with Fe monomers. Since our results indicate that the Fe dimer is clearly the favored configuration in equilibrium (i.e., at 573 K), kinetic limitations must prevent some Fe atoms finding a partner atom at 423 K. In Fig. 4(a), Fe monomers are not found in octahedral sites, indicating that the conversion to octahedral coordination must be a concerted process requiring two Fe atoms. A monomer trapped between two dimers is unable to access a second Fe atom with which to form a dimer, indicating little or no cross-row diffusion at 423 K. At 573 K, kinetic limitations are removed as no isolated Fe atoms, only Fe dimers, are observed irrespective of initial Fe coverage.

Reduced terminations of Fe_3O_4 may be important in technological and environmental applications since the stoichiometry of natural samples is often imperfect. The first observation of an "Fe dimer" was for an Fe_3O_4 film grown on Fe(001)/MgO(001),[23] thus the source of additional Fe in the buffer layer likely stabilized the partially reduced termination. Slightly Fe-rich single crystal samples may also prefer reduced terminations. We expect the reduced $Fe_3O_4(001)$ surfaces to be significantly more reactive than the distorted B-layer termination since they contain highly undercoordinated cations in the surface layer. However, since the additional Fe atoms effectively block the *n* sites, strongly preferred by adsorbates on the distorted B layer, most adsorption processes will be completely different between the surfaces. Thus care should be taken with the interpretation of data from spectroscopic techniques aimed at understanding the role of $Fe_3O_4(001)$ in geochemistry and catalysis. Finally, our results suggest that antiferromagnetic FeO forms at the $Fe_3O_4(001)$ surface on deposition. The presence of such a layer at the Fe/Fe_3O_4 interface could explain recent reports of exchange bias in the ferromagnet/ferrimagnet Fe(001)/Fe_3O_4(001) system.[38]

V. CONCLUSIONS

Reduced terminations of the $Fe_3O_4(001)$ surface were prepared by evaporating different Fe coverages onto the thermodynamically stable distorted B-layer termination at RT, 423 K, and 573 K. The step-by-step reduction observed in this manner is consistent with the theoretical phase diagram, except for the calculated phase containing a significant density of oxygen vacancies, which is not observed experimentally. The structural, electronic, and magnetic properties of the different phases are elucidated using DFT + *U* calculations. Initially, the Fe rich surfaces conform to the $(\sqrt{2} \times \sqrt{2})R45^\circ$ symmetry of the underlying substrate accommodating Fe in tetrahedral sites. The Fe-dimer surface, formed at two Fe atoms per unit cell, also exhibits $(\sqrt{2} \times \sqrt{2})R45^\circ$ symmetry. The "Fe dimers" result from a switch to octahedral cation coordination; no direct Fe-Fe bond is formed. Only at four Fe atoms per unit cell is the symmetry modified with the formation of a buckled antiferromagnetic FeO(001) surface layer on top of $Fe_3O_4(001)$.

ACKNOWLEDGMENTS

This material is based upon work supported as part of the Centre for Atomic-Level Catalyst Design, an Energy Frontier Research Centre funded by the US Department of Energy, Office of Science, Office of Basic Energy Sciences under Award No. DE-SC0001058. The authors acknowledge Professor Z. Mao and T. J. Liu (Tulane University) for the synthetic sample used in this work. G.S.P. acknowledges support from the Austrian Science Fund Project No. P24925-N20. N.M. and R.P. acknowledge funding by the German Science Foundation (SFB/TR80) and computational time at the Leibniz Rechenzentrum, Garching.

*parkinson@iap.tuwien.ac.at

[1] R. M. Cornell and U. Schwertmann, *The Iron Oxides: Structure, Properties, Reactions, Occurrences and Uses* (Wiley-VCH, New York, 2003).

[2] F. N. Skomurski, S. Kerisit, and K. M. Rosso, Geochim. Cosmochim. Acta **74**, 4234 (2010).

[3] A. Yanase and N. Hamada, J. Phys. Soc. Jpn. **68**, 1607 (1999).

[4] W. Weiss and W. Ranke, Prog. Surf. Sci. **70**, 1 (2002).

[5] P. Majewski and B. Thierry, Crit. Rev. Solid State Mater. Sci. **32**, 203 (2007).

[6] P. Tartaj, M. P. Morales, T. Gonzalez-Carreno, S. Veintemillas-Verdaguer, and C. J. Serna, Adv. Matter. **23**, 5243 (2011).

[7] T. K. Shimizu, J. Jung, H. S. Kato, Y. Kim, and M. Kawai, Phys. Rev. B **81**, 235429 (2010).

[8] K. Adib, N. Camillone, J. P. Fitts, K. T. Rim, G. W. Flynn, S. A. Joyce, and R. M. Osgood, Surf. Sci. **497**, 127 (2002).

[9] K. T. Rim *et al.*, J. Phys. Chem. B **108**, 16753 (2004).

[10] B. Stanka, W. Hebenstreit, U. Diebold, and S. A. Chambers, Surf. Sci. **448**, 49 (2000).

[11] R. Wiesendanger, I. V. Shvets, D. Burgler, G. Tarrach, H. J. Güntherodt, J. M. D. Coey, and S. Graser, Science **255**, 583 (1992).

[12] J. R. Rustad, E. Wasserman, and A. R. Felmy, Surf. Sci. **432**, L583 (1999).

[13] P. W. Tasker, J. Phys. C **12**, 4977 (1979).

[14] C. Noguera, J. Phys.: Condens. Matter. **12**, R367 (2000).

[15] N. Mulakaluri, R. Pentcheva, M. Wieland, W. Moritz, and M. Scheffler, Phys. Rev. Lett. **103**, 176102 (2009).

[16] R. Pentcheva, F. Wendler, H. L. Meyerheim, W. Moritz, N. Jedrecy, and M. Scheffler, Phys. Rev. Lett. **94**, 126101 (2005).

[17] Z. Lodziana, Phys. Rev. Lett. **99**, 206402 (2007).

[18] G. S. Parkinson, N. Mulakaluri, Y. Losovyj, P. Jacobson, R. Pentcheva, and U. Diebold, Phys. Rev. B **82**, 125413 (2010).

[19] G. S. Parkinson, Z. Novotny, P. Jacobson, M. Schmid, and U. Diebold, J. Am. Chem. Soc. **133**, 12650 (2011).

[20] K. Jordan, A. Cazacu, G. Manai, S. F. Ceballos, S. Murphy, and I. V. Shvets, Phys. Rev. B **74**, 085416 (2006).

[21] G. S. Parkinson, T. A. Manz, Z. Novotny, P. T. Sprunger, R. L. Kurtz, M. Schmid, D. S. Sholl, and U. Diebold, Phys. Rev. B **85**, 195450 (2012).

[22] G. S. Parkinson, Z. Novotny, P. Jacobson, M. Schmid, and U. Diebold, Surf. Sci. Lett. **605**, L42 (2011).

[23] N. Spiridis, J. Barbasz, Z. Lodziana, and J. Korecki, Phys. Rev. B **74**, 155423 (2006).

[24] J. Hooper, M. Zhou, Z. Mao, R. Perry, and Y. Maeno, Phys. Rev. B **72**, 134417 (2005).

[25] P. Blaha, K. Schwarz, G. K. H. Madsen, D. Kvasnicka, and J. Lutz, WIEN2k, An Augmented Plane Wave + Local Orbitals Program For Calculating Crystal Properties (Karlheinz Schwarz, Techn. Univ. Wien, Austria, 2001).

[26] J. P. Perdew, K. Burke, and M. Ernzerhof, Phys. Rev. Lett. **77**, 3865 (1996).

[27] V. I. Anisimov, I. V. Solovyev, M. A. Korotin, M. T. Czyzyk, and G. A. Sawatzky, Phys. Rev. B **48**, 16929 (1993).

[28] I. Leonov, A. N. Yaresko, V. N. Antonov, M. A. Korotin, and V. I. Anisimov, Phys. Rev. Lett. **93**, 146404 (2004).

[29] H. T. Jeng, G. Y. Guo, and D. J. Huang, Phys. Rev. Lett. **93**, 156403 (2004).

[30] N. Mulakaluri, R. Pentcheva, and M. Scheffler, J. Phys. Chem. C **114**, 11148 (2010).

[31] N. Mulakaluri and R. Pentcheva, J. Phys. Chem. C **116**, 16447 (2012).

[32] K. Reuter and M. Scheffler, Phys. Rev. B **65**, 035406 (2001).

[33] Z. Novotný, G. Argentero, Z. Wang, M. Schmid, U. Diebold, and G. S. Parkinson, Phys. Rev. Lett. **108**, 216103 (2012).

[34] G. S. Parkinson, Z. Novotny, G. Argentero, M. Schmid, J. Pavelec, R. Kosak, P. Blaha, and U. Diebold [Nature Materials (to be published)] (2013).

[35] We note that the differences in total occupation between Fe^{2+} and Fe^{3+} sites are small (0.2–0.4e) within the MT sphere, but changes in the valance can be more clearly identified in the PDOS [e.g., Fig. 6(a)] and the magnetic moments 3.54–3.75 μ_B for Fe^{2+} and 3.90–4.1 μ_B for Fe^{3+}.

[36] T. Kendelewicz, S. Kaya, J. T. Newberg, H. Bluhm, N. Mulakaluri, W. Moritz, M. Scheffler, A. Nilsson, R. Pentcheva, and G. E. Brown, Jr., J. Phys. Chem. C **117**, 2719 (2013).

[37] A. P. Grosvenor, B. A. Kobe, M. C. Biesinger, and N. S. McIntyre, Surf. Interface Anal. **36**, 1564 (2004).

[38] T. Kida, S. Honda, H. Itoh, J. Inoue, H. Yanagihara, E. Kita, and K. Mibu, Phys. Rev. B **84**, 104407 (2011).